

Relativistic Thomas-Fermi equation of state for magnetized white dwarfsSujan Kumar Roy,^{1,2,*} Somnath Mukhopadhyay,^{1,2,3,†} Joydev Lahiri,^{1,‡} and D. N. Basu^{1,2,§}¹*Variable Energy Cyclotron Centre, 1/AF Bidhan Nagar, Kolkata 700 064, India*²*Homi Bhabha National Institute, Training School Complex, Anushakti Nagar, Mumbai 400085, India*³*BITS Pilani, Hyderabad Campus, Jawahar Nagar, Kapra Mandal, Medchal District 500078 Telangana, India*

(Received 12 July 2019; published 18 September 2019)

The relativistic Feynman-Metropolis-Teller treatment of compressed atoms is extended to treat magnetized matter. Each atomic configuration is confined by a Wigner-Seitz cell and is characterized by a positive electron Fermi energy which varies insignificantly with the magnetic field. In the relativistic treatment, the limiting configuration is reached when the Wigner-Seitz cell radius equals the radius of the nucleus with a maximum value of the electron Fermi energy which cannot be attained in the presence of magnetic field due to the effect of Landau quantization of electrons within the Wigner-Seitz cell. This treatment is implemented to develop the equation of state for magnetized white dwarf stars in the presence of Coulomb screening. The mass-radius relations for magnetized white dwarfs are obtained by solving the general relativistic hydrostatic equilibrium equations using Schwarzschild metric description suitable for nonrotating and slowly rotating stars. The explicit effects of the magnetic energy density and pressure contributed by a density-dependent magnetic field are included to find the stable configurations of magnetized super-Chandrasekhar white dwarfs.

DOI: [10.1103/PhysRevD.100.063008](https://doi.org/10.1103/PhysRevD.100.063008)**I. INTRODUCTION**

Compact stars are home to the strongest magnetic fields in the Universe. Anomalous x-ray pulsars and soft gamma repeaters, which are certain classes of neutron stars called magnetars, are observed to have surface magnetic fields $\sim 10^{15}$ gauss. Moreover, a strong magnetic field of similar magnitude has been observed at the jet base of a super-massive black hole PKS 1830-211 [1]. Several magnetized white dwarfs have also been observed with surface field strengths ranging from $\sim 10^6$ – 10^9 gauss [2–4]. Such strong magnetic fields can drastically modify the equation of state (EoS) of a compact star, its structure, and stability.

A stellar magnetic field is a magnetic field generated by the motion of conductive plasma inside a star. This motion is created through convection, which is a form of energy transport involving the physical movement of material. A localized magnetic field exerts a force on the plasma, effectively increasing the pressure without a comparable gain in density. As a result, the magnetized region rises relative to the remainder of the plasma, until it reaches the star's photosphere. This creates star spots on the surface and the related phenomenon of coronal loops. Stellar magnetic fields, according to solar dynamo theory, are

caused within the convective zone of the star. The convective circulation of the conducting plasma functions like a dynamo. This activity destroys the star's primordial magnetic field and then generates a dipolar magnetic field. As the star undergoes differential rotation rotating at different rates for various latitudes, the magnetism is wound into a toroidal field of “flux ropes” that become wrapped around the star. The fields can become highly concentrated, producing activity when they emerge on the surface.

The magnetic fields of all celestial bodies are often aligned with the direction of rotation, with notable exceptions such as certain pulsars. Another feature of this dynamo model is that the currents are ac rather than dc. Their direction, and thus the direction of the magnetic field they generate, alternates more or less periodically, changing amplitude and reversing direction, although still more or less aligned with the axis of rotation. Such magnetized stars when collapse the magnetic fields of the progenitors are trapped within new compact stars. The origin of high magnetic field of the collapsed stars is due to the flux conservation in the new configuration.

Recent studies [5–8] have shown the existence of magnetized white dwarfs with masses significantly greater than the traditional Chandrasekhar's limit [9], also known as super-Chandrasekhar white dwarfs to account for the exceptionally high luminosities of the Type Ia supernovae, e.g., SN2006gz, SN2007if, SN2009dc, SN2003fg [10–14].

* sujan.kr@vecc.gov.in† somnathm@hyderabad.bits-pilani.ac.in‡ joy@vecc.gov.in§ dnb@vecc.gov.in

In these studies, the electron gas in the EoS is taken to be free, relativistic, and Landau quantized in a strong magnetic field. Hence, the masses and radii are independent of the composition of the white dwarf. Coulomb corrections to the EoS within the relativistic Feynman-Metropolis-Teller (FMT) formalism of compressed atoms at zero [15] and finite temperature [16] in the absence of magnetic field have been explored previously.

The motive of the present work is to extend the relativistic FMT treatment to study magnetized matter. We included the effects of Landau quantization of the electrons [17–20] which explicitly take care of the term coming from the magnetic field interaction with the electron magnetic moment. Thus, we obtain the changes in pressure and energy density distribution which now depend on the chosen atomic configuration contrary to the studies in Refs. [10–14]. Finally, we applied this treatment for helium, carbon, oxygen, and iron to obtain the EoS for magnetized white dwarf matter up to the limit of inverse- β decay. We solved the Tolman-Oppenheimer-Volkoff (TOV) equation, which assumes spherically symmetric configuration and hence an isotropic pressure, in order to obtain the mass-radius relationship for magnetized white dwarfs. It is worth mentioning that external magnetic field along a particular axis creates pressure anisotropy [21] which affects the mass-radius relation. For the present calculation, we found that the splitting due to pressure anisotropy is very small for smaller atomic configurations and increases with the size of the atom though never exceeding 10% of matter pressure for moderately high magnetic field even for the largest atomic configuration. The effect of pressure anisotropy has not been considered in the present work which shows that the critical mass limit, subjected to the stability against inverse- β decay, of magnetized white dwarfs increases with the magnitude of the central magnetic field. However, this increase in critical mass depends on the composition of the white dwarf as the effect is minimal for a ${}^4\text{He}$ white dwarf, and critical mass limit for ${}^{56}\text{Fe}$ white dwarf can be as high as $\sim 5 M_{\odot}$.

II. LANDAU QUANTIZATION FOR ELECTRONS IN MAGNETIC FIELD

The radius of gyration and cyclotron frequency, of an electron subjected to a uniform magnetic field B , is given by

$$r_c = \frac{m_e c v_{\perp}}{qB}; \quad \omega_c = \frac{qB}{m_e c}, \quad (1)$$

where v_{\perp} is the velocity perpendicular to the magnetic field. The Hamiltonian of the system is given by

$$H = \frac{1}{2m_e} \left(\vec{p} - \frac{q\vec{A}}{c} \right)^2, \quad (2)$$

where $\vec{B} = \nabla \times \vec{A}$ with \vec{A} being the electromagnetic vector potential. To have a magnetic field in z direction with magnitude B , one can have

$$\vec{A} = \begin{pmatrix} 0 \\ Bx \\ 0 \end{pmatrix}, \quad (3)$$

and therefore

$$H = \frac{1}{2m_e} \left[p_x^2 + \left(p_y - \frac{qBx}{c} \right)^2 + p_z^2 \right]. \quad (4)$$

Using cyclotron frequency $\omega_c = \frac{qB}{m_e c}$, one obtains

$$H = \frac{p_x^2}{2m_e} + \frac{1}{2} m_e \omega_c^2 \left(x - \frac{\hbar k_y}{m_e \omega_c} \right)^2 + \frac{p_z^2}{2m_e}, \quad (5)$$

the first two terms represent a harmonic oscillator shifted at $x_0 = \frac{\hbar k_y}{m_e \omega_c}$ with $\hbar k_y$ being \hat{p}_y eigenvalues. Hence, the energy eigenvalues are

$$E_{\nu, p_z} = \nu \hbar \omega_c + \frac{p_z^2}{2m_e}, \quad \nu = n + \frac{1}{2} + s_z, \quad (6)$$

where $n = 0, 1, 2, \dots$ is the harmonic oscillator quantum number and ν is called the Landau quantum number. Zeeman effect [22] gets included through s_z term. The dynamically generated anomalous magnetic moment in massless QED [23] is insignificant [24] for charged fermions for EoS of a magnetized dense medium since Lande's g -factor $\cong 2(1 + \frac{\alpha}{2\pi})$ is negligibly different from 2 for electrons, where α is the fine structure constant. Hence, for the lowest Landau level ($\nu = 0$), the spin degeneracy $g_{\nu} = 1$ (since only $n = 0$, $s_z = -\frac{1}{2}$ is allowed) and for higher Landau levels ($\nu \neq 0$), $g_{\nu} = 2$ (as $s_z = \pm \frac{1}{2}$ both are allowed). Relativistically, E_{ν, p_z} is given by [25]

$$E_{\nu, p_z} = [p_z^2 c^2 + m_e^2 c^4 (1 + 2\nu B_D)]^{\frac{1}{2}}, \quad (7)$$

where $B_D = B/B_c$ with B_c given by $\hbar \omega_c = \hbar \frac{eB_c}{m_e c} = m_e c^2 \Rightarrow B_c = \frac{m_e^2 c^3}{e\hbar} = 4.414 \times 10^{13}$ gauss. The Fermi energy E_F is given by

$$E_F^2 = p_F^2(\nu) c^2 + m_e^2 c^4 (1 + 2\nu B_D), \quad (8)$$

where $p_F(\nu)$ is the Fermi momentum. The upper limit of Landau level ν_m can be found from

$$\nu \leq \frac{\epsilon_F^2 - 1}{2B_D} \Rightarrow \nu_m = \frac{\epsilon_{Fmax}^2 - 1}{2B_D}, \quad (9)$$

where $\epsilon_F = E_F/m_e c^2$. At zero temperature, the number density of electrons is given by

$$n_e = \frac{2B_D}{(2\pi)^2 \lambda_e^3} \sum_{\nu=0}^{\nu_m} g_\nu x_F(\nu), \quad (10)$$

where $\lambda_e = \frac{\hbar}{m_e c}$ is the Compton wavelength for electron, $x_F(\nu) = \frac{p_F(\nu)}{m_e c}$ and

$$\epsilon_F = [x_F^2(\nu) + 1 + 2\nu B_D]^{\frac{1}{2}} \quad (11)$$

$$\Rightarrow x_F(\nu) = [\epsilon_F^2 - (1 + 2\nu B_D)]^{\frac{1}{2}}. \quad (12)$$

The electron energy density is given by

$$\begin{aligned} \epsilon_e &= \frac{2B_D}{(2\pi)^2 \lambda_e^3} \sum_{\nu=0}^{\nu_m} g_\nu \int_0^{x_F(\nu)} E_{\nu, p_z} d\left(\frac{p_z}{m_e c}\right) \\ &= \frac{B_D m_e c^2}{2\pi^2 \lambda_e^3} \sum_{\nu=0}^{\nu_m} g_\nu (1 + 2\nu B_D) \psi\left(\frac{x_F(\nu)}{(1 + 2\nu B_D)^{1/2}}\right), \end{aligned} \quad (13)$$

where

$$\begin{aligned} \psi(z) &= \int_0^z (1 + y^2)^{1/2} dy \\ &= \frac{1}{2} \left[z\sqrt{1 + z^2} + \ln\left(z + \sqrt{1 + z^2}\right) \right]. \end{aligned} \quad (14)$$

The pressure of the electron gas is given by

$$\begin{aligned} P_e &= n_e^2 \frac{d}{dn_e} \left(\frac{\epsilon_e}{n_e} \right) = n_e E_F - \epsilon_e \\ &= \frac{B_D m_e c^2}{2\pi^2 \lambda_e^3} \sum_{\nu=0}^{\nu_m} g_\nu (1 + 2\nu B_D) \eta\left(\frac{x_F(\nu)}{(1 + 2\nu B_D)^{1/2}}\right), \end{aligned} \quad (15)$$

where

$$\begin{aligned} \eta(z) &= z\sqrt{1 + z^2} - \psi(z) \\ &= \frac{1}{2} \left[z\sqrt{1 + z^2} - \ln\left(z + \sqrt{1 + z^2}\right) \right]. \end{aligned} \quad (16)$$

III. THE RELATIVISTIC FEYNMAN-METROPOLIS-TELLER TREATMENT IN PRESENCE OF MAGNETIC FIELD

For the extension of FMT formalism in the presence of magnetic field, a compressed atom as a Wigner-Seitz cell consisting of a finite size nucleus with mass number A and atomic number Z at the center of the cell and completely degenerate relativistic electron gas embedded in a strong

magnetic field is considered. As described in the preceding section, electrons being charged particles occupy Landau quantized states in a magnetic field B and the maximum number of particles per Landau level per unit area is $\frac{eB(2s+1)}{\hbar c}$. The Fermi energy E_F of the ν th Landau level in the external magnetic field B in z direction and under the influence of Coulomb potential $V(r)$ can now be given by

$$E_F = [p_F^2(\nu)c^2 + m_e^2 c^4 (1 + 2\nu B_D)]^{\frac{1}{2}} - m_e c^2 - eV(r), \quad (17)$$

where the Fermi energy is constant over a compressed Wigner-Seitz cell. A constant number density distribution of protons $n_p(r)$ is assumed which is confined within nuclear radius $R_c = r_0 A^{\frac{1}{3}} = \Delta \lambda_\pi Z^{\frac{1}{3}}$, with $\lambda_\pi = \frac{\hbar}{m_\pi c}$ being the Compton wavelength for pion of rest mass m_π and hence can be given by $n_p(r) = \frac{Z}{\frac{4}{3}\pi R_c^3} \theta(R_c - r)$.

Defining $\hat{V}(r) = eV(r) + E_F$, from Eq. (17), $p_F(\nu) = \sqrt{\hat{V}^2 + 2\hat{V}m_e c^2 - 2\nu B_D m_e^2 c^4}$ and from the condition $p_F^2 \geq 0$, the upper limit of Landau level ν_m can be obtained as $\nu_m = \frac{\hat{V}^2 + 2\hat{V}m_e c^2}{2B_D m_e^2 c^4}$.

Using Landau quantization, the number density of electrons under the influence of Coulomb screening is, therefore, given by

$$n_e(r) = \frac{2B_D}{(2\pi)^2 \lambda_e^3} \sum_{\nu=0}^{\nu_m} g_\nu x_F(\nu)$$

$$\text{where } p_F(\nu)c = \left[(\hat{V}^2 + 2m_e c^2 \hat{V}) \left(1 - \frac{\nu}{\nu_m} \right) \right]^{\frac{1}{2}}, \quad (18)$$

with $x_F(\nu) = \frac{p_F(\nu)c}{m_e c^2}$ as before. The overall Coulomb potential $V(r)$ can be obtained by solving the Poisson equation

$$\begin{aligned} \nabla^2 V(r) &= -4\pi e [n_p(r) - n_e(r)] \\ \Rightarrow \nabla^2 \hat{V}(r) &= -4\pi e^2 [n_p(r) - n_e(r)]. \end{aligned} \quad (19)$$

Introducing the dimensionless quantities $x = \frac{r}{\lambda_\pi}$ and $\chi(x) = r \frac{\hat{V}(r)}{\hbar c} = x \frac{\hat{V}(x)}{m_e c^2}$, Eq. (19) can be rewritten as

$$\begin{aligned} \frac{1}{x} \frac{d^2 \chi(x)}{dx^2} &= -\frac{3\alpha\theta(x_c - x)}{\Delta^3} + \frac{2e^2 B_D}{\pi \hbar c} \left(\frac{m_\pi}{m_e} \right) \left(\frac{\lambda_\pi}{\lambda_e} \right)^3 \\ &\times \sum_{\nu=0}^{\nu_m} g_\nu \left[\left(1 - \frac{\nu}{\nu_m} \right) \left\{ \left(\frac{\chi}{x} \right)^2 + 2 \left(\frac{m_e}{m_\pi} \right) \left(\frac{\chi}{x} \right) \right\} \right]^{\frac{1}{2}}. \end{aligned} \quad (20)$$

The electrostatic potential and the number density distribution of electrons can be obtained by solving Eq. (20) with the boundary conditions $\chi(0) = 0$ and $\chi'(x_{WS}) = \chi(x_{WS})/x_{WS}$, where x_{WS} is the dimensionless radius of

the Wigner-Seitz cell. The first boundary condition follows from the fact that potential cannot become infinite at the center of the cell, while the second boundary condition implies the charge neutrality which must ensure charge number conservation $Z = \int_0^{r_{\text{WS}}} 4\pi n_e(r) r^2 dr$ as well as $\chi(x_{\text{WS}}) \geq 0$ that preserves the basic assumption of FMT approach that a compressed Wigner-Seitz cell is characterized by a positive Fermi energy.

IV. THE EQUATION OF STATE

Once the relativistic FMT is solved for a compressed atom in the presence of magnetic field, the EoS can be constructed. The kinetic energy density including the electronic rest mass within the Wigner-Seitz cell is given by

$$\varepsilon_k(x) = \frac{B_D m_e c^2}{2\pi^2 \lambda_\pi^3} \sum_{\nu=0}^{\nu_m} g_\nu (1 + 2\nu B_D) \psi \left(\frac{x_F(\nu)}{(1 + 2\nu B_D)^{1/2}} \right) \quad (21)$$

at radius (dimensionless) $r(x)$ from the center of the cell. The dependence on x , unlike the previous case (Sec. II), is due to inclusion of Coulomb screening in Eq. (18). The total kinetic energy E_k of the cell excluding the electronic rest mass can be calculated as

$$E_k = 4\pi \lambda_\pi^3 \int_{x_c}^{x_{\text{WS}}} x^2 [\varepsilon_k(x) - n_e(x) m_e c^2] dx, \quad (22)$$

where $x_c = \frac{R_c}{\lambda_\pi}$ is the dimensionless radius of the nucleus resting at the center of the cell. As the calculations will be performed up to the onset of inverse- β decay, the electrons are absent inside the nucleus and the integration is performed from x_c .

The total potential energy E_c of the cell can be evaluated using

$$\begin{aligned} E_c &= 4\pi \lambda_\pi^3 \int_0^{x_{\text{WS}}} x^2 [n_p(x) - n_e(x)] eV(x) dx \\ \Rightarrow E_c &= -4\pi \lambda_\pi^3 \int_{x_c}^{x_{\text{WS}}} x^2 n_e(x) eV(x) dx \\ &= -4\pi \lambda_\pi^3 m_\pi c^2 \int_{x_c}^{x_{\text{WS}}} x n_e(x) \chi(x) dx + E_F Z, \end{aligned} \quad (23)$$

where the lower limit of the integration is changed to x_c since in the forthcoming calculations, while calculating energy density, measured atomic masses will be used implying that electronic rest mass and Coulomb energy contribution due to nucleus will be accounted and the term n_p is dropped since protons are not present beyond x_c . It is, therefore, obvious that in Eq. (22) electronic rest mass is subtracted to avoid double counting.

The energy density ε can now be given by

$$\varepsilon = \frac{E_k + E_c + M(A, Z) c^2}{\frac{4\pi}{3} r_{\text{WS}}^3} + \frac{B^2}{8\pi}, \quad (24)$$

where $M(A, Z)$ is atomic mass of the uncompressed atom, and the last term accounts for the magnetic contribution to the energy density. The pressure P is simply given by

$$P = \frac{B_D m_e c^2}{2\pi^2 \lambda_\pi^3} \sum_{\nu=0}^{\nu_m} g_\nu (1 + 2\nu B_D) \eta \left(\frac{x_F(\nu)}{(1 + 2\nu B_D)^{1/2}} \right) + \frac{B^2}{24\pi}, \quad (25)$$

but it should be evaluated at the cell boundary, and the last term accounts for the magnetic contribution to the pressure.

V. RESULTS AND DISCUSSION

Recently, there have been some important calculations for masses and radii of magnetized white dwarfs using nonrelativistic Lane-Emden equation and assuming a constant magnetic field throughout the star. These calculations yield masses up to 2.3–2.6 M_\odot [5] which are significantly greater than the Chandrasekhar limit. However, because of the structure of the Lane-Emden equation, pressure arising due to a constant magnetic field does not contribute to masses or radii whereas in the general relativistic TOV [26,27] equation, it is not the case. Moreover, the EoS needed to be fitted to a polytropic form. In order to derive a mass limit for magnetized white dwarfs (similar to the mass limit of $\sim 1.4 M_\odot$ obtained by Chandrasekhar [9] for nonmagnetic white dwarfs), the same authors, under certain approximations, have been able to reduce the EoS to a polytropic form with index $1 + 1/n = 2$ for which analytic solution of Lane-Emden equation exists [$\theta(\xi) = \sin \xi / \xi$ where $\rho = \rho_c \theta^n$ with ρ and ρ_c being density and central density, respectively], and avoiding the energy density $\varepsilon_B = \frac{B^2}{8\pi}$ and pressure $P_B = \frac{1}{3} \varepsilon_B$ arising due to magnetic field by assuming it to be constant throughout, they were able to set a mass limit of 2.58 M_\odot [6,28]. The masses and radii of white dwarfs have been calculated by solving the general relativistic TOV equation both for nonmagnetic and magnetized white dwarfs using the exact EoS without resorting to fit it to a polytropic form [8].

In this present work, to find out the critical mass limit for magnetized white dwarfs the general relativistic hydrostatic equilibrium equation (TOV) has been solved for the EoS obtained up to the density for onset of inverse- β decay. The critical density $\rho_{\text{crit}}^{\beta, \text{unif}}$ for the onset of inverse- β decay within the approximation of uniform electron density distribution is given by

TABLE I. The onset of inverse beta decay instability for ${}^4\text{He}$, ${}^{12}\text{C}$, ${}^{16}\text{O}$, and ${}^{56}\text{Fe}$. The experimental inverse- β decay energies $\epsilon_\beta(Z)$ have been taken from Table 1 of [29]. The corresponding critical density for the uniform electron density model $\rho_{\text{crit}}^{\beta,\text{unif}}$ is calculated using Eq. (26), while the critical density $\rho_{\text{crit}}^{\beta,\text{relFMT}}$ under the magnetic field for the relativistic FMT case is calculated by the condition that E_F given by Eq. (17) reaches asymptotically the inverse- β decay threshold energy $\epsilon_\beta(Z)$ whose numerical values are taken from [30]; see also [31].

Decay channel	$\epsilon_\beta(Z)$ (MeV)	$\rho_{\text{crit}}^{\beta,\text{relFMT}}(5B_c)$ (g cm $^{-3}$)	$\rho_{\text{crit}}^{\beta,\text{unif}}$ (g cm $^{-3}$)
${}^4\text{He} \rightarrow {}^3\text{H} + n \rightarrow 4n$	20.596	1.368×10^{11}	1.37×10^{11}
${}^{12}\text{C} \rightarrow {}^{12}\text{B} \rightarrow {}^{12}\text{Be}$	13.370	3.812×10^{10}	3.88×10^{10}
${}^{16}\text{O} \rightarrow {}^{16}\text{N} \rightarrow {}^{16}\text{C}$	10.419	1.785×10^{10}	1.89×10^{10}
${}^{56}\text{Fe} \rightarrow {}^{56}\text{Mn} \rightarrow {}^{56}\text{Cr}$	3.695	1.139×10^9	1.14×10^9

$$\rho_{\text{crit}}^{\beta,\text{unif}} = \frac{A_r M_u}{Z 3\pi^2 (\hbar c)^3} [(\epsilon_\beta(Z))^2 + 2m_e c^2 \epsilon_\beta(Z)]^{3/2}, \quad (26)$$

where A_r is the measured mass in atomic mass unit, M_u is the atomic mass unit expressed in MeV, and $\epsilon_\beta(Z)$ is the energy to ignite the inverse- β decay. The experimental energies for inverse- β decay are listed in Table I. The values of the critical densities $\rho_{\text{crit}}^{\beta,\text{unif}}$ have been calculated using Eq. (26) for the decays given in Table I. The A_r values used for ${}^4\text{He}$, ${}^{12}\text{C}$, ${}^{16}\text{O}$, and ${}^{56}\text{Fe}$ are 4.003, 12.01, 16.00, and 55.84, respectively. The EoS calculations for magnetic field B_D have been performed up to maximum (critical) densities restricted by the condition that E_F given by Eq. (17) reaches asymptotically the inverse- β decay threshold energy $\epsilon_\beta(Z)$. The critical densities $\rho_{\text{crit}}^{\beta,\text{relFMT}}$ for $B_D = 5B_c$ have also been provided in Table I. The inverse- β decay threshold energies have been assumed to be independent of magnetic field. Under this assumption, the values of $\rho_{\text{crit}}^{\beta,\text{relFMT}}$ do not differ much from zero magnetic field since the change in Fermi energy E_F has a weak dependence on magnetic field.

If a charged particle having charge q moves with velocity v perpendicular to an external magnetic field B , the equilibrium is established through $\frac{mv^2}{r} = qvB$, i.e., the magnetic field $B = \frac{mv}{qr}$ implies higher the magnetic field lower the radius of the trajectory of the particle. This simple logic applies to the atomic configuration subjected to magnetic field as well. Hence, it is expected in the light of the above logic that the radius of a particular cell decreases with the magnetic field. As described earlier in Sec. III in the presence of magnetic field, the relativistic FMT treatment has been applied to study the changes in the Wigner-Seitz cell and it has been found that the density increases with magnetic field, though the variation of density with magnetic field is not as fast as $\rho \propto B^3$ which can be accounted for the Coulomb screening considered

under FMT treatment as well as the three-dimensional configuration of Wigner-Seitz cell. On the other hand, in the presence of magnetic field, the Landau quantization in the perpendicular plane becomes effective as described in Sec. II.

From Eq. (9), it is clear that ν_m depends on E_F and B_D . As Fermi energy increases with density, ν_m is expected to increase with density and decrease with the magnetic field. Both Figs. 9 and 10 show that ν_{max} decreases with increasing magnetic field, implying the fact that under high magnetic field the gap between successive Landau levels increases. Again, an atomic configuration subjected to higher compression will be of higher density and hence will be characterized by higher Fermi energy. So, the ν_{max} of higher density configuration will be larger than ν_{max} of lower density as can be understood from the comparison of Figs. 9 and 10. In FMT treatment, each compressed atomic configuration is characterized by a constant Fermi energy. However, an electron closer and tightly bound to the nucleus carries more kinetic energy it implies that for a particular magnetic field, the Landau-level quantum number should be greater near the nucleus. The dilute and distant electrons are more vulnerable to the effects of a magnetic field. Hence, higher the quantization effect and lower the ν_{max} toward the surface of the cell. These are depicted in each of the curves in Figs. 9 and 10. Considering all these facts, it can be inferred that the atoms which are most compressed are least affected by the magnetic field, as can be seen from the comparisons of the Figs. 1–8 that the differences in the distributions are reduced in the higher density domain. As the compact stars are believed to be formed from the stellar collapse, an atom subjected to higher compression (corresponding to higher density) is supposed to have a higher magnetic field and this can be connected with the simple formula $\frac{B_1}{B_2} = \left(\frac{\rho_1}{\rho_2}\right)^{\frac{2}{3}}$, where $B_1(B_2)$ and $\rho_1(\rho_2)$ are the atomic configuration's magnetic field and density, respectively. 1.53×10^7 gm cm $^{-3}$ density is used for the calculations in Fig. 9, and 4.96×10^8 gm cm $^{-3}$ density is used for calculations in Fig. 10 for the same kind of atom. As $\left(\frac{4.96 \times 10^8}{1.53 \times 10^7}\right)^{\frac{2}{3}} \sim 10$, it is expected that the ν_{max} values for $1B_c$ in Fig. 9 will be replicated in the ν_{max} values for $10B_c$ in Fig. 10.

The higher the value of ν_m in Eq. (9) and lower the gap between two successive Landau levels $\hbar \frac{eB}{m_e c}$, lesser will be the quantization effect on the system. In the presence of magnetic field $B \rightarrow 0$, the gap between two successive Landau levels vanishes and the energy spectrum becomes continuum. Hence, the lowest magnetic field electron distribution function will closely resemble the no magnetic field electron distribution. This can be seen from Figs. 7 and 8 where it is found that the $1B_c$ magnetic field curve almost overlaps with the $0B_c$ curve. However, as we increase the magnetic field, the quanta $\hbar \frac{eB}{m_e c}$ increases

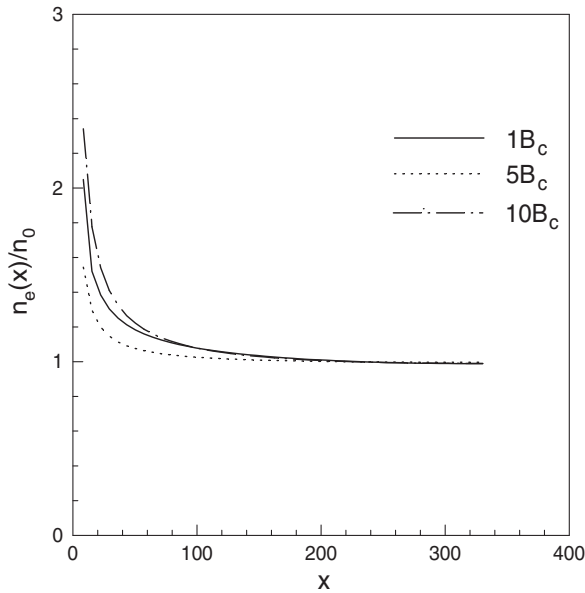


FIG. 1. Plots for $n_e(x)/n_0$ as functions of dimensionless radial coordinate x at density $1.53 \times 10^7 \text{ gm cm}^{-3}$ for ${}^4\text{He}$.

and hence more is the effect of quantization on the electron density distribution. However, with increasing the density, the Fermi energy E_F of the atomic configuration increases which in turn increases the ν_m , thereby reducing the quantization effect, and hence the deviation in the electronic distribution from no magnetic field case gets reduced with higher density and this can be confirmed from the comparison between Figs. 7 and 8. Figures 1 and 2 show the electronic distributions of ${}^4\text{He}$ under different magnetic field strengths, and Figs. 3–6 represent the same for ${}^{12}\text{C}$

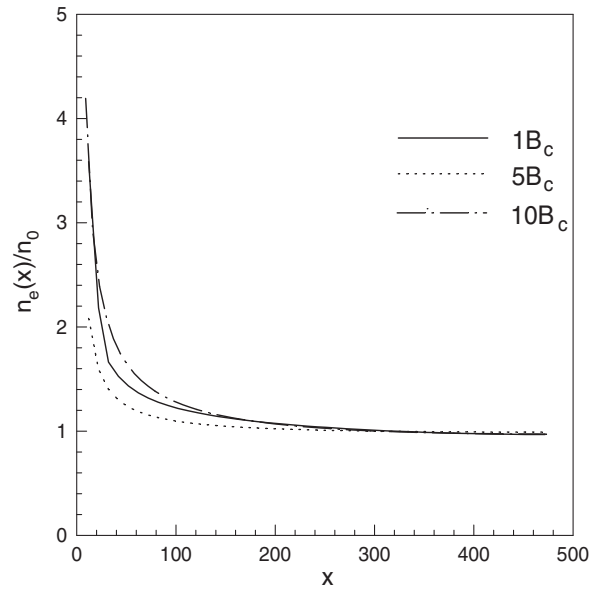


FIG. 3. Plots for $n_e(x)/n_0$ as functions of dimensionless radial coordinate x at density $1.53 \times 10^7 \text{ gm cm}^{-3}$ for ${}^{12}\text{C}$.

and ${}^{16}\text{O}$, respectively. As it has been observed that ν_m is a function of the radial coordinate (Figs. 9 and 10), we can expect a small hump in the electronic distributions when calculated in the presence of magnetic field. In Figs. 1–6, the electronic distributions have been plotted for different atoms and their different densities. A close look at these figures enables one to observe the small humps unlike the no magnetic field case where the electronic distribution is totally smooth. This factor is further confirmed by calculating the first derivative of the density distribution function where the effects of these humps are more severe.

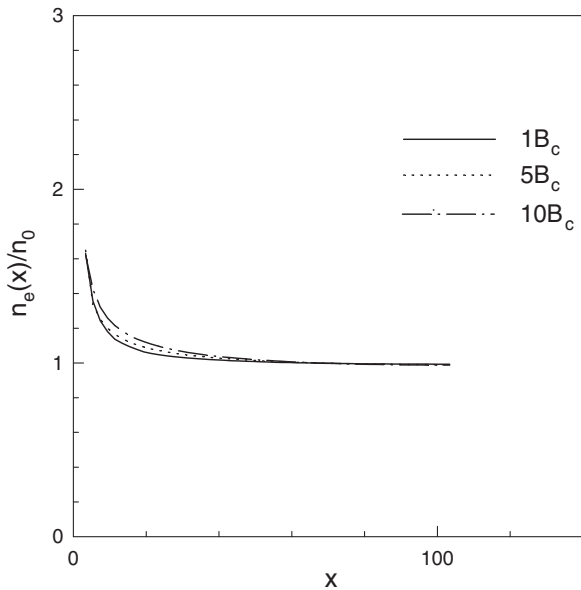


FIG. 2. Plots for $n_e(x)/n_0$ as functions of dimensionless radial coordinate x at density $4.96 \times 10^8 \text{ gm cm}^{-3}$ for ${}^4\text{He}$.

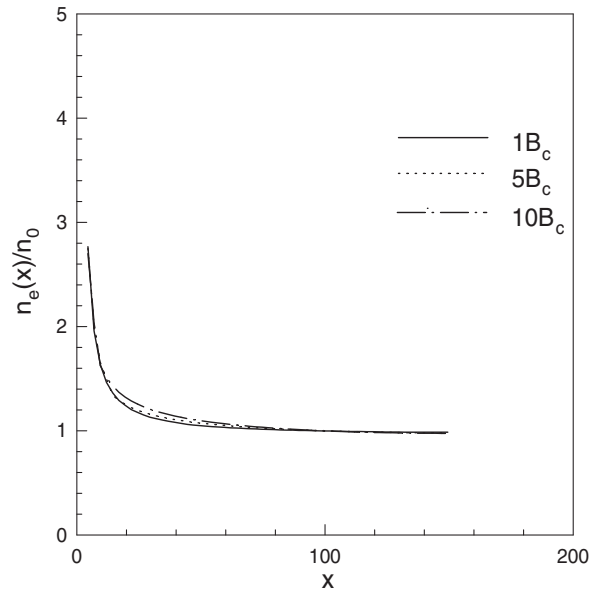


FIG. 4. Plots for $n_e(x)/n_0$ as functions of dimensionless radial coordinate x at density $4.96 \times 10^8 \text{ gm cm}^{-3}$ for ${}^{12}\text{C}$.

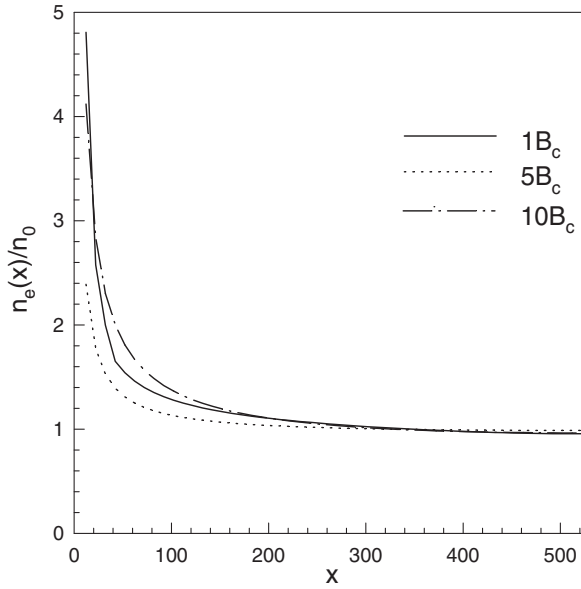


FIG. 5. Plots for $n_e(x)/n_0$ as functions of dimensionless radial coordinate x at density $1.53 \times 10^7 \text{ gm cm}^{-3}$ for ^{16}O .

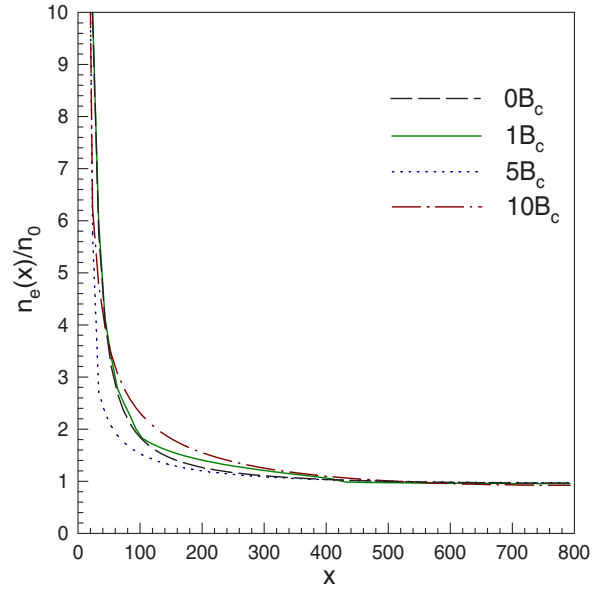


FIG. 7. Plots for $n_e(x)/n_0$ as functions of dimensionless radial coordinate x at density $1.53 \times 10^7 \text{ gm cm}^{-3}$ for ^{56}Fe .

In Figs. 1–8, plots for $n_e(x)/n_0$ as functions of dimensionless radial coordinate x of Wigner-Seitz cell have been shown for ^4He , ^{12}C , ^{16}O , and ^{56}Fe under the influence of three different magnetic fields and for two different densities where n_0 is number density assuming uniform distribution inside. In Figs. 9 and 10, plots for maximum Landau levels ν_{max} as functions of dimensionless radial coordinate x of Wigner-Seitz cell have been shown for ^{56}Fe under the influence of three different magnetic fields and for two different densities.

Compact stars are believed to be formed from the stellar collapse of main sequence heavy stars. At the end of their stellar evolution when the thermal pressure becomes incapable of balancing the gravitational pull, it collapses down till the Fermi degeneracy pressure of electrons grows so much that it halts the collapse. This provides the star a stable configuration, when the outward degeneracy pressure balances the inward gravitational pull, which can be yielded from the equation of hydrostatic equilibrium, i.e., TOV equation [26,27]. The pressure gradient $\frac{dP}{dr}$ from TOV

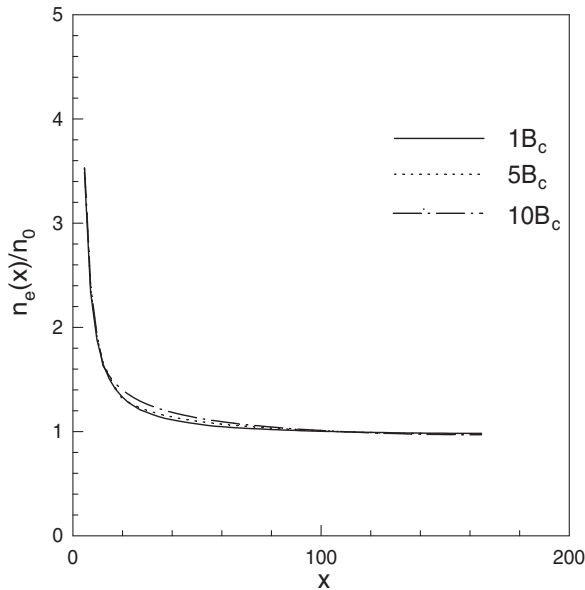


FIG. 6. Plots for $n_e(x)/n_0$ as functions of dimensionless radial coordinate x at density $4.96 \times 10^8 \text{ gm cm}^{-3}$ for ^{16}O .

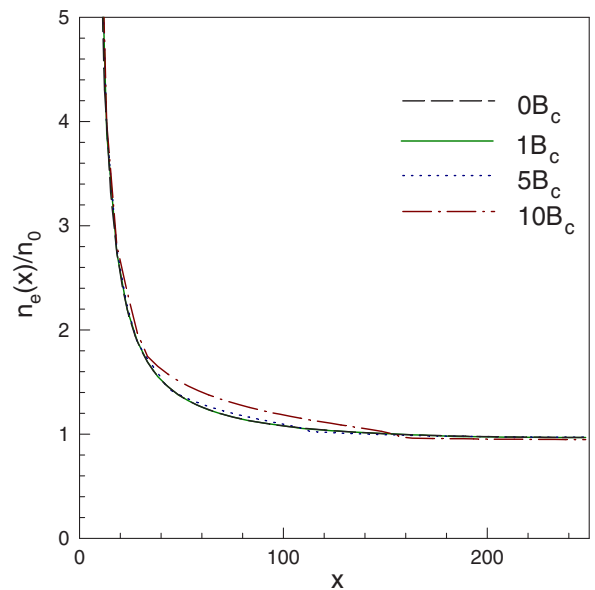


FIG. 8. Plots for $n_e(x)/n_0$ as functions of dimensionless radial coordinate x at density $4.96 \times 10^8 \text{ gm cm}^{-3}$ for ^{56}Fe .

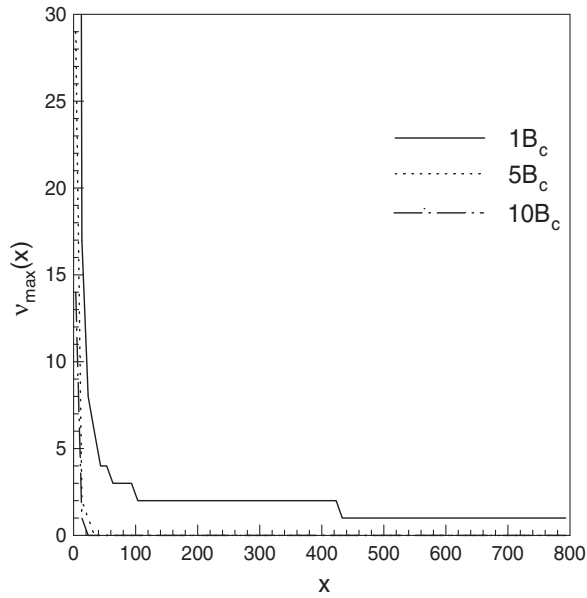


FIG. 9. Plots for ν_{\max} as functions of dimensionless radial coordinate x at density $1.53 \times 10^7 \text{ gm cm}^{-3}$ for ^{56}Fe .

can be intuitive to understand the configuration of such a collapsed star. As relativistically or nonrelativistically, the electron Fermi degeneracy pressure contributed from the constituting matter of the star can be expressed as $P(r) = \text{constant} \times \rho(r)^\gamma$. Hence, the $\rho = \text{constant}$ cannot be a possible solution for the interior of such a star made up of highly compressed degenerate matter. On the other hand, as every term in the right-hand side of the pressure gradient equation is positive, $\frac{dP}{dr}$ must be ≤ 0 . The equality holds for the matter at infinity, i.e., on the surface of the star as is

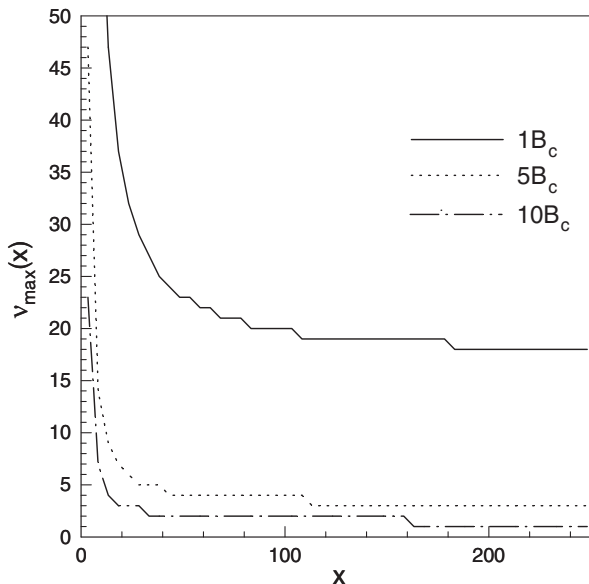


FIG. 10. Plots for ν_{\max} as functions of dimensionless radial coordinate x at density $4.96 \times 10^8 \text{ gm cm}^{-3}$ for ^{56}Fe .

obvious from the equation. Hence, the TOV equation governs a configuration with pressure, maximum at the center of the star, which gradually approaches 0 on the surface implying a similar density distribution. But when the star collapses, it is supposed that the magnetic field of the progenitor is trapped into it. So, the magnetic field of the collapsed star is nothing but how the flux is getting conserved in the new configuration. Hence, to preserve the flux conservation, the magnetic field of the new configuration can be connected with the progenitor's one by the relation $\frac{B}{B_{\text{prog}}} = \left(\frac{\rho}{\rho_{\text{prog}}}\right)^{\frac{2}{3}}$, where $B(B_{\text{prog}})$ and $\rho(\rho_{\text{prog}})$ are the white dwarf's magnetic field (progenitor star) and density (progenitor star), respectively. If for simplicity we assume a constant distribution of magnetic field over the progenitor star, the surface magnetic field gets fixed in the range of 10^6 – 10^9 gauss confirmed from observations [2–4]. As the density at the center of the white dwarf can be as high as $\sim 10^9$ – 10^{10} times, the density near the surface, central magnetic field can go as high as $\sim 10^{12}$ – 10^{15} gauss.

However, if we take a magnetic field profile depending on the density through the equation $\frac{B_D}{B_s} = \left(\frac{\rho}{\rho_s}\right)^{\frac{2}{3}}$, where B_D (in units of B_c) is the magnetic field at density ρ , B_s (in units of B_c) is the surface magnetic field, it would provide a steep magnetic field. But in the presence of magnetic field, since in general relativity every source of energy is a source of gravitation, the gravitational pull must be balanced by the combined effects of magnetic field and electron degeneracy pressure. Then at the center of the star such magnetic field ($\sim 10^{15}$ – 10^{16} gauss) would provide a huge magnetic pressure which may lead to local instabilities. If the magnetic pressure at center turns out to be really high to dominate the gravitational field, then the magnetic pressure may drive the collapsed matter to exhibit unstable convection flow; therefore, one can expect expulsion of such huge central magnetic field in a stable configuration. Second, the huge magnetic field can lead to production of particles in the system and the corresponding energy extraction can reduce the central magnetic field. Ultimately, we infer that such a magnetic field profile cannot be sustained rather a magnetic field profile having flatness near the center and the surface is preferred over such a configuration.

On the basis of the above discussion, the actual calculations have been performed with varying magnetic field including the effects of energy density and pressure arising due to magnetic field in a general relativistic framework. The variation of magnetic field [32] inside the white dwarf is taken to be of the form

$$B_D = B_s + B_0[1 - \exp\{-\beta(\rho/\rho_0)^\gamma\}], \quad (27)$$

where ρ_0 is taken as $\rho(r=0)/10$ and β, γ are constants. Once central magnetic field is fixed, B_0 can be determined

from the above equation. We choose constants $\beta = 0.8$ and $\gamma = 0.9$ to ensure flatness of the field near the surface and the center. Nevertheless, the magnetic field profile could have been taken with different parameter values as far as no local instability incurs. It would not alter the gross result by much unless the central magnetic field varies significantly and can be applied safely subjected to the virial condition of stability that the magnetic energy never exceeds the gravitational binding energy [33]. The maximum limit of central magnetic field strength of the configuration given by Eq. (27), therefore, must be chosen carefully owing to all these stability criteria and for the present calculations it is kept $10B_c$, which is 4.414×10^{14} gauss, near to the lower of the maximum limit, as suggested by N. Chamel *et al.* [33,34]. The surface magnetic field $B_s \sim 10^9$ gauss is estimated by observations.

The configurations having predominantly high nuclear binding energy are ${}^4\text{He}$, ${}^{12}\text{C}$, ${}^{16}\text{O}$, and ${}^{56}\text{Fe}$ with 7.08, 7.68, 7.73, and 8.80 MeV per nucleon, respectively. In the binding energy per nucleon versus mass number curve, ${}^{56}\text{Fe}$ is at the maximum whereas the other three nuclides occupy three peaks in the curve. Therefore, in the present calculation, these four types of configurations have been considered. We assumed that a progenitor star after running out of its nuclear fuel collapses to finally form a white dwarf from either of these abovementioned materials. If the collapse can ignite further nuclear fission, the white dwarf can again act as a living star and go under the same process of stellar evolution till the configuration of ${}^{56}\text{Fe}$ is reached as no further evolution is possible beyond this because this is the most stable nuclide having the maximum binding energy per nucleon.

For different types of atoms of same density, the Wigner-Seitz cell radius is $R_{\text{WS}} \propto A_r^{1/3}$. Hence, more the atomic number, more is the trapped magnetic flux for the same magnetic field profile. For simplicity, if one assumes a constant magnetic field distribution which after a gravitational collapse forms a magnetic field profile as used in Eq. (27), then it is quite obvious that to form an iron white dwarf, which is able to encompass a huge number of flux compared to ${}^4\text{He}$, ${}^{12}\text{C}$, or ${}^{16}\text{O}$, a larger amount of mass of progenitor star is to be collapsed than the other configurations. On the other hand, it may as well be formed that after many stellar evolution cycles, it may be able to hold such kind of a magnetic field profile consistent with a large amount of magnetic flux encompassing for iron cell. This factor in turn reflects a possibility of getting considerably higher critical masses for iron white dwarf than that for helium, carbon, or oxygen white dwarfs. It can be envisaged that higher the central magnetic field, higher the trapped magnetic flux implying a larger collapse of the progenitor. Hence, white dwarfs can be predicted by larger critical masses with the increasing magnetic field. These factors can be confirmed from the figures. In Figs. 11 and 12, masses and radii of

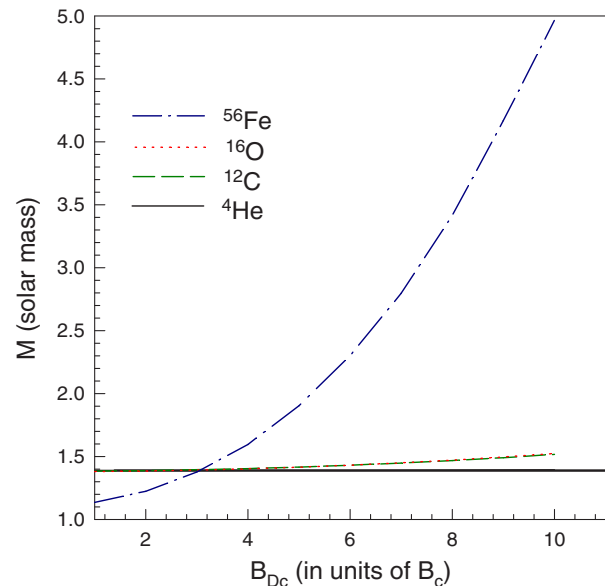


FIG. 11. Plots for maximum (critical) masses of magnetized white dwarfs as a function of central magnetic field.

magnetized white dwarfs are shown as functions of the central magnetic field. The present calculation estimates that the effect is minimal for a ${}^4\text{He}$ white dwarf and exceeds slightly the Chandrasekhar's limit for ${}^{12}\text{C}$ and ${}^{16}\text{O}$ white dwarfs while for ${}^{56}\text{Fe}$ the maximum mass can be as high as $\sim 5 M_\odot$. These results are quite useful in explaining the peculiar, overluminous type Ia supernovae that do not conform to the traditional Chandrasekhar mass limit.

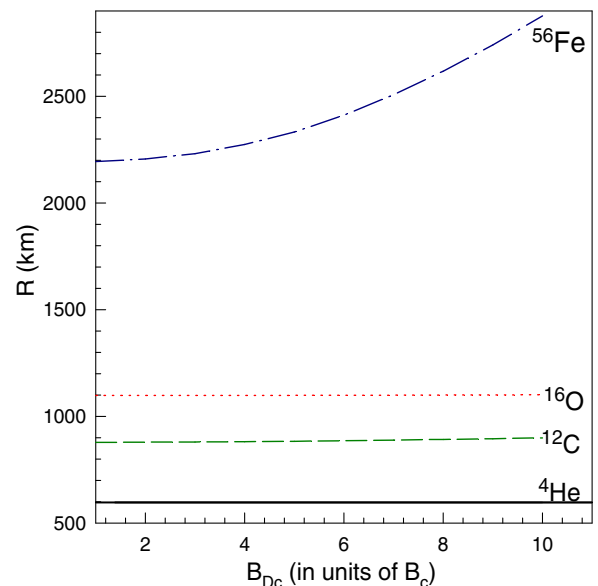


FIG. 12. Plots for radii of maximum (critical) masses of magnetized white dwarfs as a function of central magnetic field.

VI. SUMMARY AND CONCLUSION

In summary, we have considered each compressed atom to be confined within a Wigner-Seitz cell with nucleus at its center surrounded by relativistic degenerate electrons. The effect of strong magnetic field is incorporated by modifying the density of states of electrons due to Landau quantization. The Coulomb screening substantially alters the number density of electrons from the uniform one which reduces the effective degeneracy pressure at the cell boundary causing modification of EoS of the white dwarf matter. Any source of energy gravitates according to general relativity. Hence, the presence of magnetic field contributes additively to energy density and pressure. The masses and radii of magnetized white dwarfs, with a density dependent magnetic field profile which is high at the center, have been calculated by solving the TOV equations. We find that the critical mass limit, subjected to the stability against inverse- β decay, of such white dwarfs increase with the magnitude of the central magnetic field. However, this increase in critical mass depends on the mass number of atoms. The effect is minimal for a

${}^4\text{He}$ white dwarf and exceeds largely the Chandrasekhar's limit for ${}^{56}\text{Fe}$ white dwarfs which can be as high as $\sim 5 M_{\odot}$.

To date there are about ~ 250 magnetized white dwarfs with well-determined fields [4] and over ~ 600 if objects with no or uncertain field determination [2,3] are also included. Surveys such as the Sloan Digital Sky Survey, Hamburg Quasar Survey, and the Cape Survey have discovered these magnetized white dwarfs. The complete samples show that the field distribution of magnetized white dwarfs is in the range 10^3 – 10^9 gauss, which basically provides the surface magnetic fields. However, the central magnetic field strength, which is presumably unobserved by the above observations, could be several orders of magnitude higher than the surface field. In fact, it is the central magnetic field which is crucial for super-Chandrasekhar magnetized white dwarfs. However, the softening of the EoS accompanying the onset of electron captures and pycnonuclear reactions in the core of these stars can lead to local instabilities which set an upper limit to the magnetic field strength at the center of the star, ranging from 10^{14} to 10^{16} gauss depending on the core [33] composition.

-
- [1] I. Marti-Vidal, S. Muller, W. Vlemmings, C. Horellou, and S. Aalto, *Science* **348**, 311 (2015).
 - [2] S. O. Kepler, I. Pelisoli, S. Jordan, S. J. Kleinman, D. Koester, B. Külebi, V. Pecanha, B. G. Castanheira, A. Nitta, J. E. S. Costa, D. E. Winget, A. Kanaan, and L. Fraga, *Mon. Not. R. Astron. Soc.* **429**, 2934 (2013).
 - [3] S. O. Kepler, I. Pelisoli, D. Koester, G. Ourique, S. J. Kleinman, A. D. Romero, A. Nitta, D. J. Eisenstein, J. E. S. Costa, B. Külebi, S. Jordan, P. Dufour, P. Giommi, and A. Rebassa-Mansergas, *Mon. Not. R. Astron. Soc.* **446**, 4078 (2015).
 - [4] L. Ferrario, D. de Martino, and B. T. Gänsicke, *Space Sci. Rev.* **191**, 111 (2015).
 - [5] U. Das and B. Mukhopadhyay, *Phys. Rev. D* **86**, 042001 (2012).
 - [6] U. Das and B. Mukhopadhyay, *Phys. Rev. Lett.* **110**, 071102 (2013).
 - [7] R. Nityananda and S. Konar, *Phys. Rev. D* **89**, 103017 (2014).
 - [8] S. Mukhopadhyay, D. Atta, and D. N. Basu, *Romanian reports in Physics* **69**, 101 (2017).
 - [9] S. Chandrasekhar, *Mon. Not. R. Astron. Soc.* **95**, 207 (1935).
 - [10] D. A. Howell *et al.*, *Nature (London)* **443**, 308 (2006).
 - [11] R. A. Scalzo *et al.*, *Astrophys. J.* **713**, 1073 (2010).
 - [12] M. Hicken, P. M. Garnavich, J. L. Prieto, S. Blondin, D. L. DePoy, R. P. Kirshner, and J. Parrent, *Astrophys. J.* **669**, L17 (2007).
 - [13] M. Yamanaka *et al.*, *Astrophys. J.* **707**, L118 (2009).
 - [14] J. M. Silverman, M. Ganeshalingam, W. Li, A. V. Filippenko, A. A. Miller, and D. Poznanski, *Mon. Not. R. Astron. Soc.* **410**, 585 (2011).
 - [15] M. Rotondo, J. A. Rueda, R. Ruffini, and S.-S. Xue, *Phys. Rev. D* **84**, 084007 (2011).
 - [16] S. M. de Carvalho, M. Rotondo, J. A. Rueda, and R. Ruffini, *Phys. Rev. C* **89**, 015801 (2014).
 - [17] A. A. Sokolov and I. M. Ternov, *Synchrotron Radiation* (Pergamon, Oxford, 1968).
 - [18] L. D. Landau and E. M. Lifshitz, *Quantum Mechanics*, 3rd ed. (Pergamon, Oxford, 1977).
 - [19] V. Canuto and J. Ventura, *Fundam. Cosm. Phys.* **2**, 203 (1977).
 - [20] P. Mészáros, *High Energy Radiation from Magnetized Neutron Stars* (University of Chicago, Chicago, 1992).
 - [21] E. J. Ferrer and A. Hackebill, *Phys. Rev. C* **99**, 065803 (2019).
 - [22] P. Zeeman, *Nature (London)* **55**, 347 (1897).
 - [23] E. J. Ferrer and V. de la Incera, *Nucl. Phys.* **B824**, 217 (2010).
 - [24] E. J. Ferrer, V. de la Incera, D. Manreza Paret, A. Prez Martinez, and A. Sanchez, *Phys. Rev. D* **91**, 085041 (2015).
 - [25] D. Lai and S. L. Shapiro, *Astrophys. J.* **383**, 745 (1991).
 - [26] R. C. Tolman, *Phys. Rev.* **55**, 364 (1939).
 - [27] J. R. Oppenheimer and G. M. Volkoff, *Phys. Rev.* **55**, 374 (1939).
 - [28] J. M. Dong, W. Zuo, P. Yin, and J. Z. Gu, *Phys. Rev. Lett.* **112**, 039001 (2014).

- [29] G. Audi, A. H. Wapstra, and C. Thibault, *Nucl. Phys.* **A729**, 337 (2003).
- [30] A. H. Wapstra and K. Bos, *At. Data Nucl. Data Tables* **19**, 175 (1977).
- [31] S. L. Shapiro and S. A. Teukolsky, *Black Holes, White Dwarfs, and Neutron Stars: The Physics of Compact Objects* (Wiley-Interscience, New York, 1983).
- [32] D. Bandyopadhyay, S. Chakrabarty, and S. Pal, *Phys. Rev. Lett.* **79**, 2176 (1997).
- [33] N. Chamel, A. F. Fantina, and P. J. Davis, *Phys. Rev. D* **88**, 081301(R) (2013).
- [34] N. Chamel, Zh. K. Stoyanov, L. M. Mihailov, Y. D. Mutafchieva, R. L. Pavlov, and Ch. J. Velchev, *Phys. Rev. C* **91**, 065801 (2015).